Journal of MATERIALS RESEARCH

Article
DOI:10.1557/s43578-023-01144-0

3D PRINTING FOR MEDICAL APPLICATIONS

FOCUS ISSUE

Obtaining biocompatible polymeric scaffolds loaded with calcium phosphates through the digital light processing technique

Carolina Duque[1], Carlos Andrés Gómez-Tirado[1], Sebastián Ocampo[1], Liliana María Arroyave-Muñoz[2], Luz Marina Restrepo-Munera[2], Andrés Felipe Vásquez[3], Alex Ossa[4], Claudia García[1,a)]

[1] Universidad Nacional de Colombia, Medellín, Colombia
[2] Universidad de Antioquia, Medellín, Colombia
[3] Newstetic, Guarne, Colombia
[4] School of Applied Sciences and Engineering, Universidad Eafit, Medellín, Colombia
[a)] Address all correspondence to this author. e-mail: cpgarcia@unal.edu.co

Received: 12 May 2023; accepted: 8 August 2023

In the present work, scaffolds with gyroid TPMS geometry were obtained from a commercial resin of acrylic nature loaded with 0.5% and 1% w/V of calcium phosphate nanoparticles through DLP. The scaffolds obtained presented Young's Modulus between 300 and 400 MPa, which makes them suitable for bone applications. The surface treatment by oxygen plasma carried out on the scaffolds resulted in a notable improvement in the wettability of the surfaces, which favours cell adhesion on the surface of the materials. The in vitro bioactivity assay conducted on the resin/calcium phosphate particles composite material showed that an apatitic layer forms on the surface of the samples from the third day of exposure to simulated body fluid (SBF), indicating that the composite material has in vitro bioactive behaviour. Biological tests demonstrated that the material is not cytotoxic and favours cell adhesion and that the gyroid geometry promotes cell proliferation.

Introduction

The incidence of fractures in the population is considered to present one peak in young people and another in older adults. In the young population, fractures are generally associated with significant trauma, which typically occur in long bones and being more frequently in men than in women. In the case of older adults, one in two women and one in five men will experience a fracture that will have a lasting impact on their lives due to diseases such as osteoporosis [1]. In the year 2000, there were an estimated 9 million new fractures caused by osteoporosis, of which 1.6 million were in the hip, 1.7 million in the forearm, and 1.4 million were clinically diagnosed vertebral fractures. [1–3]. Currently, bone fractures, degenerative diseases, and various neoplastic diseases are the most common clinical problems associated with the bone and skeletal system [4]. Most of these cases need to be treated with surgery, requiring the use of implantable devices with custom sizes and shapes, with a latent risk for bacterial infections, the main cause of bone implant failure [5, 6]. In response to the need for substitute manufacturing methods for bone grafts, additive manufacturing technologies have been used to create structures that can be used as replacements that mimic the characteristics of the extracellular matrix of the affected organs or tissues [7, 8]. Tissue engineering enables strategies to be used for the deposition of cells in natural or artificial structures, known as scaffolds and their subsequent implantation [9].

Scaffolds must have high porosity and well-distributed and interconnected pores to facilitate cell penetration, nutrient diffusion, vascular growth, and other processes. Triply Periodic Minimal Surfaces (TPMS) are well suited for use in scaffold manufacture since they have the optimal relationship between stiffness and porosity levels to facilitate cell growth [10]. Geometric characteristics of scaffolds such as surface curvature, pore size, and shape have been shown to have a major influence

on scaffold cell performance [8]. These structures show high fluid permeability, which may be beneficial for nutrient delivery in vivo [11].

Additive manufacturing (AM), generally called 3D printing, has emerged as an alternative to address the need to manufacture substitutes for bone grafts or scaffolds, with morphological and size characteristics that can not be achieved through conventional process. AM allows great geometric freedom, facilitating the creation of complex surgical pieces or implants without the need to use additional molds or assemblies [12, 13]. In addition, it allows variables such as pore size, shape, and interconnectivity to be controlled [14, 15]. Stereolithography (SLA) and digital light processing (DLP) are notable among the available 3D printing techniques due to their precision and resolution [16, 17]. They enable control over the internal macro/microarchitecture, degree of porosity, and organization of pores, as well as providing freedom in terms of customized composition, design, and shape of the fabricated geometries [7]. Additionally, they offer low manufacturing costs [16] due to reduced printing time requirements [18] and the ability to work with various composite materials utilizing commercial raw materials [13]. These processes consist of the solidification of a resin or photopolymer that is initially in a liquid state, using a laser beam or the digital projection of light for images, with a very specific light frequency and power, normally in the UV spectrum. The light follows the surface and its contour successively layer by layer, solidifying the material until the final piece is obtained [13].

The component materials of the resins used in stereolithography are mixtures between polyacrylates and epoxy macromers. However, in recent years, resins have been developed that include biodegradable and biocompatible biomaterials, which make it easier for them to adapt to contact with living tissue without adverse effects [16]. Nonetheless, the characteristics of the scaffolds that are intended to be used in bone must include a structure similar to the extracellular matrix in order to promote cell adhesion, proliferation, and differentiation, as well as not generating a toxic environment and providing adequate load-bearing support [17]. For this reason, when designing a scaffold produced by SLA or DLP, it is important to consider not only specific morphologies or structures but also the addition of materials to the photocurable resins, such as nanoparticles, to facilitate the best biological and mechanical conditions [16].

Several materials have been studied as potential additions to photocurable resins to be used for these technologies, with a view to improving certain characteristics of the polymeric material such as mechanical, optical, and electrical properties. These include bioactive glass, zirconia, alumina, and calcium phosphates [16, 18–20]. Calcium phosphates have high mechanical resistance and good bioactivity, and for this reason, they have been used as reinforcements in biocompatible resins to increase cell proliferation and adhesion and promote bone repair [16, 21]. Calcium phosphates have shown great potential through their excellent biocompatibility, good performance, degradation capacity [22, 23], good mechanical stability, and wear and corrosion resistance [24]. They are considered an ideal material for the repair of bone defects because they have a composition that is very similar to that of natural bone tissue [22, 23]. Hydroxyapatite is a primary mineral component of teeth and bones that is recognized for its ability to interconnect with neighbouring tissues and promote cell attachment within its pores, it also has osteoinductive properties [24, 25]. Other calcium phosphates also present high biocompatibility and excellent biodegradability. The latter property is especially important as it allows the ceramic material to be absorbed and promotes the creation of new bone tissue [23, 26], favouring the adhesion and proliferation of bone cells, in turn leading to mineralization of the surface [19, 27].

This study aims to create scaffolds in the form of gyroid TPMS through the digital light processing (DLP) technique, using a commercial biocompatible resin with the addition of low amounts of calcium phosphate nanoparticles synthesized in the laboratory. The physical–chemical and biological behaviour of this material was evaluated, with the aim to demonstrating its potential for use in tissue engineering.

Results and discussion

Ceramic powder characterization

The calcium phosphate particles used to make the suspensions in the resin were synthesized through the self-combustion method. The results of the tests carried out to characterize the particles obtained can be found in some works carried out previously [28–30]. The calcium phosphates present were hydroxyapatite (HAP) and β-tricalcium phosphate and calcium pyrophosphate was found in a minority. With the thermal treatment, the crystallization of the majority phases improved, and the pyrophosphate phase disappeared. These materials have excellent biocompatibility, bioactivity, osteoconductivity, and compositional similarities to bone [14, 31]. The prior characterizations carried out on the powders obtained by self-combustion and heat-treated at 800 °C found the presence of aggregates of approximately 5 μm in diameter, composed of nanoparticles with a granular or spherical morphology [28]. The grain size of the particles, obtained by statistical counting of 200 of them, was approximately 42.9 nm ± 1.12 nm. It is important to know and control the size of the particles and of the aggregates that can be formed, since for 3D printing using the stereolithography (STL) or digital light processing (DLP) technique, the average size of the ceramic particles or aggregates that are added to the polymer must be smaller than the thickness of the layer. Otherwise,

the vertical resolution of the piece could be affected [32]. In this case, since the particles were approximately in the order of nanometers in size and the aggregates were smaller than the layer size used, the print resolution was not affected.

Resin characterization

The viscosity of the liquid resin without ceramic filler at 25 °C was 952 mPa·s. Typically, higher viscosity resins that can be used for uncomplicated stereolithography printing reach approximately 5 Pa·s [13]. In addition, for a resin-particle suspension to be appropriate for SLA or DLP processes, its viscosity must be relatively low so that the material in the vat of the machine self-levels during printing. Resins loaded with solid materials must have viscosities of less than 3000 mPa·s, which corresponds to loads of less than 50 vol% [32]. Both conditions are met in this work. The resin used has a viscosity of less than 5 Pa·s and is thus considered a low viscosity resin; and the ceramic loads used of 0.5 and 1% w/V of calcium phosphate particles were very low, which facilitates DLP printing of the prepared suspension.

The FTIR result for the resin after being cured is presented in Fig. 1(a), showing a range between 500 and 4000 cm^{-1}. There is quite a high level of similarity between the spectrum of the uncured resin (not showed)) and that of the cured resin [Fig. 1(a)], so there is no evidence of the formation of functional groups due to the ultraviolet light-curing process. The band that occurs at 1717 cm^{-1} was attributed to the stretching vibrations of the C=O bonds, the band at 1638 cm^{-1} is characteristic of C=C bonds and the band at 832 cm^{-1} is characteristic of C–H bonds. All three bands are inherent to acrylic groups [33–38] indicating that the unpigmented *Portux Print 3D Model* resin used in this work contains mainly acrylic oligomers.

The curve corresponding to the thermogravimetric analysis (TGA) of the resin pellets manufactured by DLP printing is presented in Fig. 1(b). The range for the thermal decomposition of the polymer was 260–470 °C. The TGA curve shows that mass losses are minimal between 21 and 300 °C, with the most significant decrease being observed between 300 and 470 °C. Thereafter, the rate of mass change decreased steadily, until reaching a decrease of almost 100%. The characteristics of the resin used in this work are consistent with those obtained in other studies[26, 26, 27, 39–41] and are typical of acrylic resins.

Scaffolds characterization

The scaffolds obtained after the DLP printing of the polymer-ceramic composite and the post-curing treatment can be observed in Fig. 2(a–c). Cylindrical scaffolds with dimensions of 10 × 5 mm (diameter x height) with gyroid geometry were successfully obtained, which are very similar to the CAD design, presented in Fig. 2(d). Macroscopically, no differences in morphology were observed between the scaffolds obtained with the different percentages of particles. The scaffolds have interconnected porosity and curved walls. A significant difference can be perceived in the opacity of each scaffold, with 0CaP being the brightest and most translucent [Fig. 2(a)] and 1CaP the opaquest [Fig. 2(c)]. These changes in hue indicate the presence of different amounts of particles in the scaffolds.

Figure 3(a–f) shows the SEM images obtained in the scaffolds. The regularity and precision of the surfaces of the scaffolds obtained with DLP technology can be noticed. In Fig. 3(b), lines transversal to the surface of the scaffold can be observed, which represent the different layers of the printing process. No protruding pores or irregularities are observed between the layers or on the surface they form. Figures 3(c–f) present images of the scaffolds made with 05CaP and 1CaP respectively, in which it is possible to distinguish the ceramic particles. The difference between the concentration of these on the surface of the 05CaP scaffold [Fig. 3(d)] and the 1CaP scaffold [Fig. 3(f)] is significant, the latter having the higher number of particles and

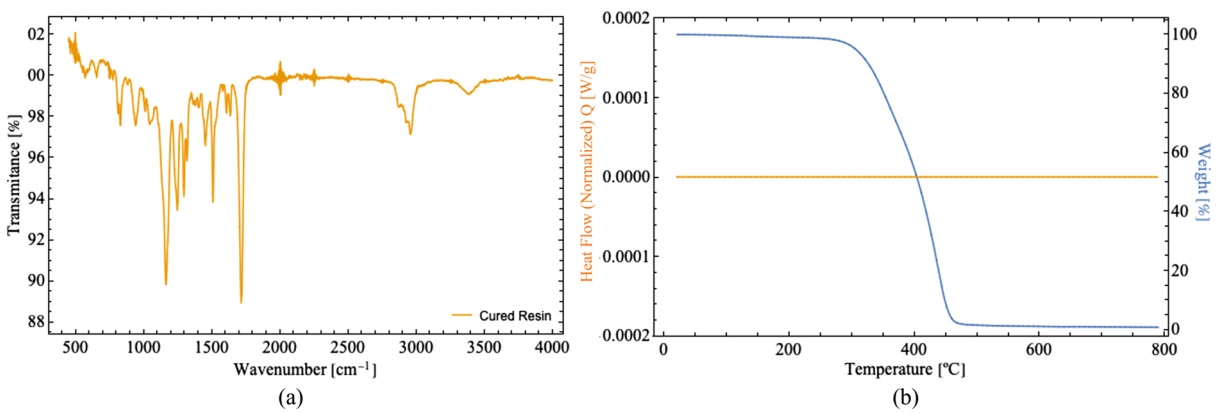

Figure 1: (a) FTIR spectra of the commercial Resin without particles post-curing, (b) Thermogravimetric curve of commercial resin.

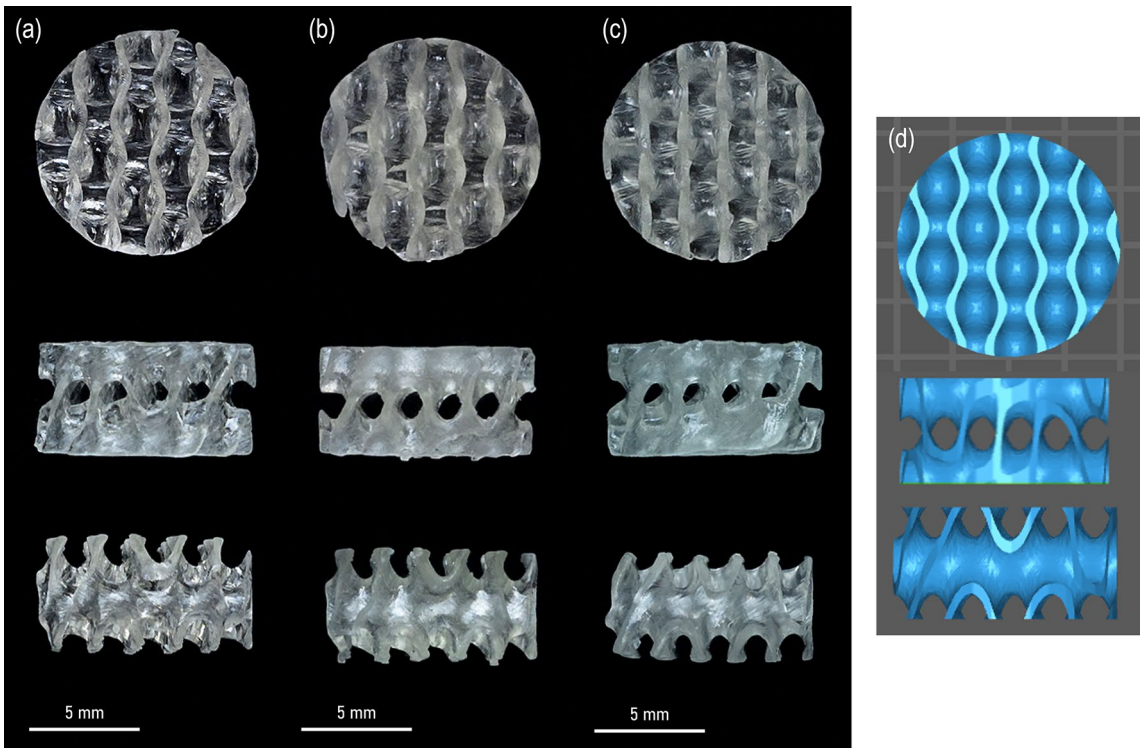

Figure 2: Digital photographs of the Scaffolds obtained by DLP printing and CAD model. Top and side views of (a) 0CaP (b) 05CaP (c) 1CaP and (d) CAD model.

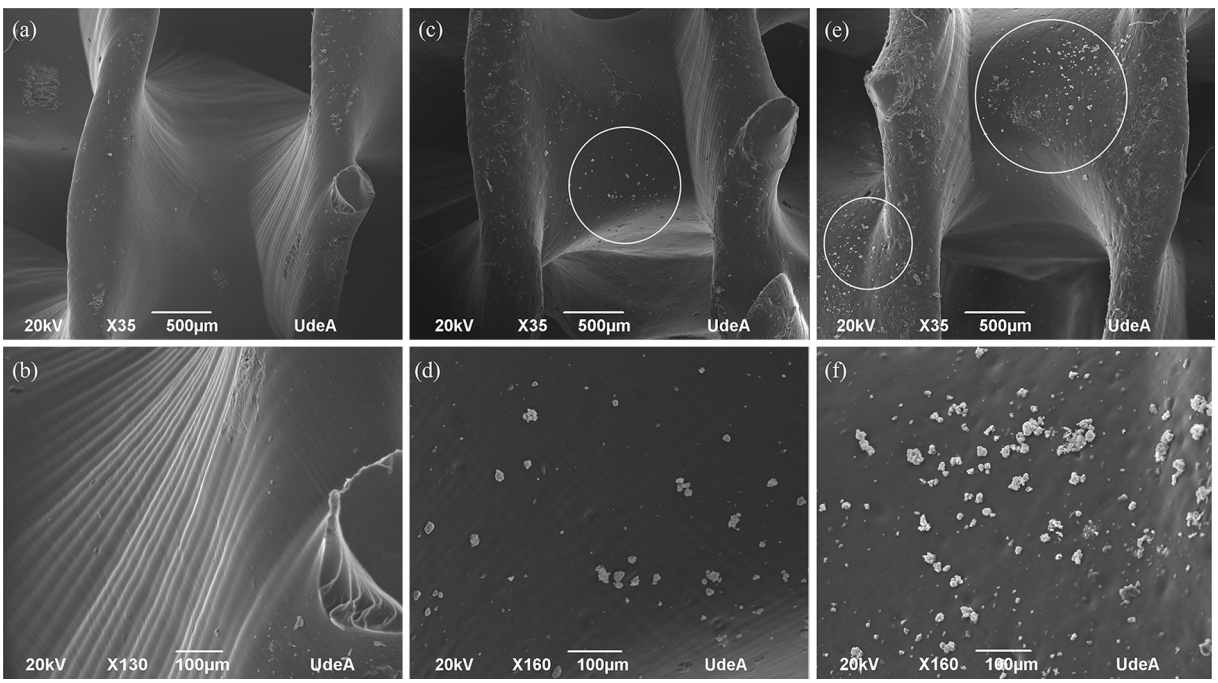

Figure 3: Scanning Electron Microscopy (SEM) images of scaffolds obtained by DLP printing. (a–b) 0CaP scaffolds. (c–d) 05CaP scaffolds. (e–f) 1CaP scaffolds.

aggregates. The EDS carried out on one of the particles observed through scanning electron microscopy, corroborated that they are formed by phosphorus (P) and calcium (Ca), confirming what was observed for the previously synthesized CaP nanoparticles added to the resin.

Mechanical behavior

Figure 4 shows the mechanical results obtained for the samples tested. Figure 4(a) shows the stress–strain results obtained for the scaffolds with 0CaP, 05CaP and 1CaP. After an initial deformation, corresponding to the adjustment of the sample to the testing plates, can be seen a linear elastic response used to calculate the Young's modulus of the samples. Soon after, the sample reach its maximum followed by a sudden drop in load due to the failure of the sample. The maximum stress reached by the sample was used as a measure of the compressive strength of the samples. The stress–strain results for the all the samples showed a similar response. Figures 4(b) and (c) show the results for the compressive strength and Young's modulus for the different scaffolds obtained by DLP. There are no significant differences in the compressive strength [Fig. 4(b)] between the scaffolds with and without ceramic filler, demonstrating that the aggregated particles are well adhered to the resin and don´t cause defects that decrease the strength of the scaffolds. There are also no significant differences between Young's modulus of the specimens with and without ceramic load or between the two evaluated ceramic loads [Fig. 4(c)], although a slight tendency of Young's modulus towards higher values is noted for the scaffolds with ceramic load (05CaP and 1CaP) indicating that the presence of ceramic particles adds stiffness to the polymeric material. Young's Modulus values between 300 and 400 MPa indicate that scaffolds can be used for bone biomedical applications [42].

Contact angle

Figure 5 shows the average contact angle measurements made of the 10 mm diameter tablets obtained by DLP with and without plasma treatment. The average results of these measurements are found in Fig. 5(c). The pellets obtained with 0CaP, 05CaP, and 1CaP that were not subjected to surface treatment with plasma present average contact angles between 80° and 90°. This indicates that the resin has hydrophobic behavior, which is normal in resins of an acrylic nature [43]. However, there is a notable decrease for the tablets of the 3 types of samples that were treated with oxygen plasma, with average angles between 47.7° and 55°. This indicates that the surface treatment carried out favors the interaction of the samples with surrounding aqueous liquids and thus cell adhesion. Oxygen plasma modification promotes the formation of free radicals that can act as binding sites for active species [44]. Thus, the incorporation of different polar groups such as hydroxyl (–C–OH), carbonyl (C=O) or carboxyl (–OH–C=O) [45, 46] that favor hydrogen bonds could be induced, allowing the accommodation of water droplets [42]. No significant differences were observed between the contact angles measured in the samples treated with the 0CaP, 05CaP, and 1CaP plasma, so it can be assumed that the CaP particles do not alter the

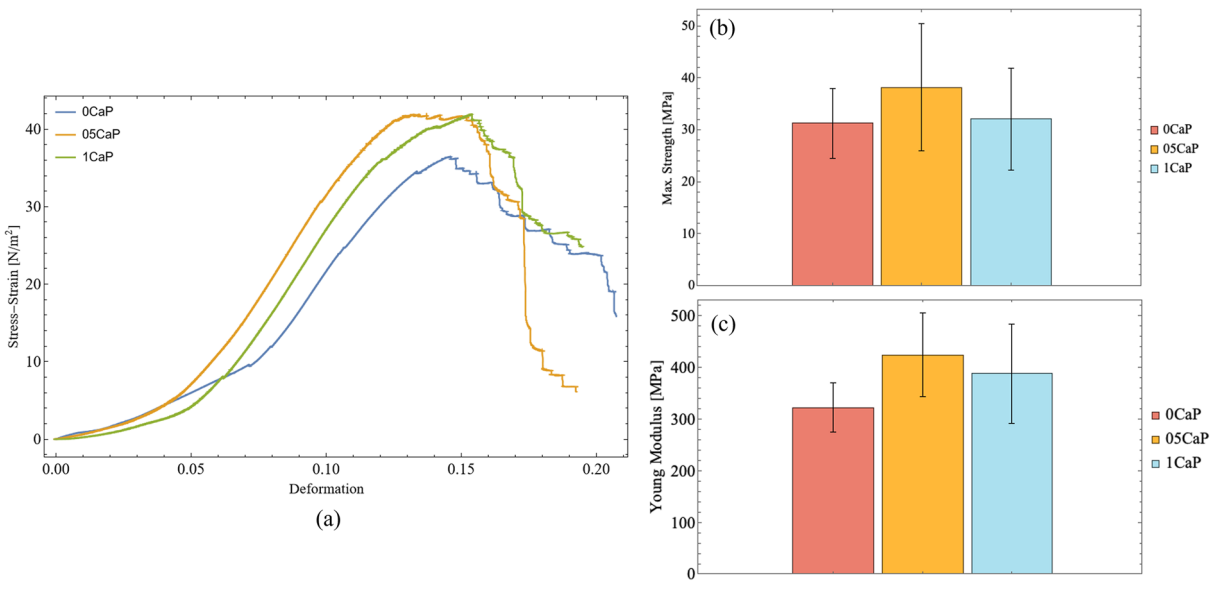

Figure 4: Mechanical behaviour of the 0CaP, 05CaP, and 1CaP scaffolds. (a) Stressstress-strain curves obtained for the scaffolds with 0CaP, 05CaP and 1CaP (b) compressive strength (c) Young's modulus.

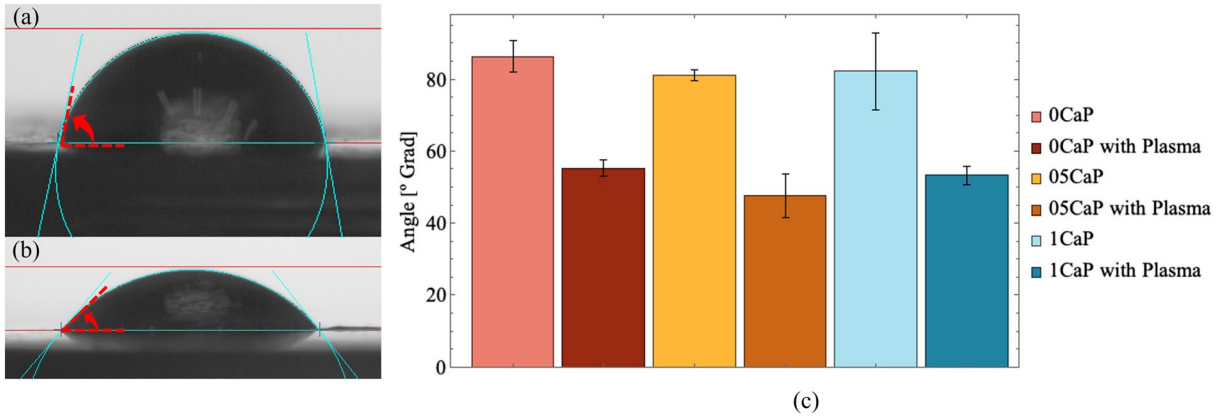

Figure 5: Contact angles. (a) Contact angle of 05CaP pellet without plasma treatment. (b) Contact angle of 05CaP pellet with plasma treatment. (c) Average measurements of pellets 0CaP, 05CaP and 1CaP.

relationship of the surface of the printed bodies with water molecules.

In vitro bioactivity test

According to the methodology described by Kokubo et al. [23, 47–49] and Ramila et al. [44], the 10 mm diameter pills with plasma treatment with and without particles were immersed in SBF for 18 days, in order to evaluate the formation of apatitic phases on their surface. An apatite layer was formed on the surface of the 05CaP and 1CaP pills treated with oxygen plasma after being immersed in simulated body fluid (SBF), while no such layer was formed on the 0CaP pellets. The samples loaded with nanoparticles are potentially bioactive in vitro due to the presence of calcium phosphate particles, which promote reactivity with the SBF. The first appearance of apatite on the surface of the samples is recorded after 3 days of immersion in SBF, and this increases with time until day 18, with no significant differences between the reactivity of the 05CaP and 1CaP samples. Figure 6 shows the surface of the 05CaP (a-b) and 1CaP (c-d) pills after three days of exposure to SBF. In the images, the apatite depositions are indicated with white arrows. Figure 6(e–f) shows the EDS analysis that was performed on one of the deposited particles, corroborating the presence of phosphorus and calcium in the particles. The calculated Ca/P ratio from the EDS data is 2,3. This ratio could correspond to initial precipitations of TTCP (tetracalcium phosphate) with a Ca/P ratio of approximately 2.00, which is highly soluble [50]. The phosphorus (P) peak is shielded by the gold (Au) peak from the coating made prior to observation. FTIR spectra of

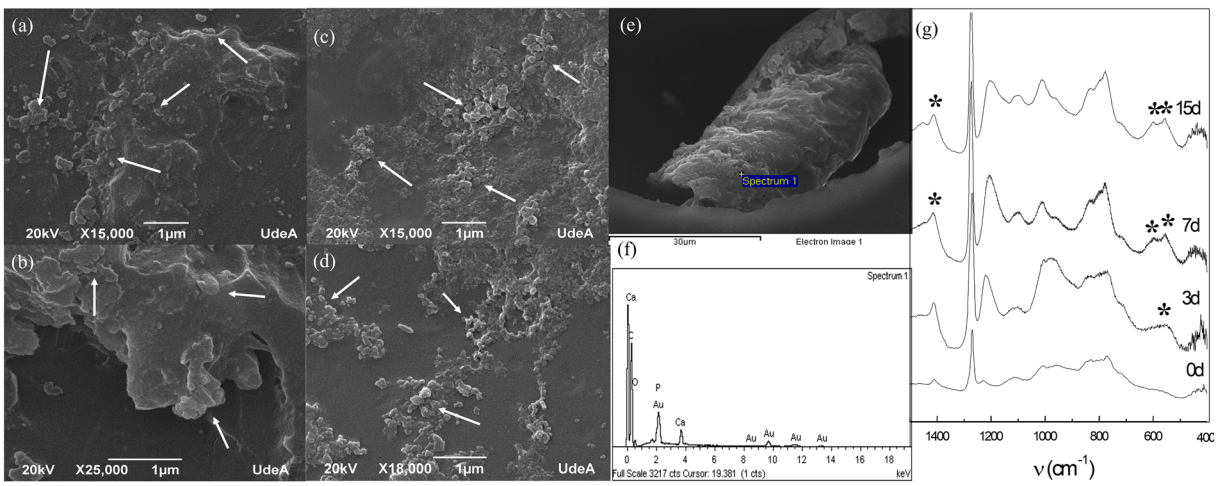

Figure 6: SEM images of (a-b) 05CaP and (c-d) 1CaP pellets treated with oxygen plasma after 3 days immersed in SBF. Depositions of calcium phosphates are indicated by arrows. (e–f) EDS analysis of the deposited calcium phosphate particles (g) FTIR Spectra of the depositions after 0, 3 7 and 15 days of immersion in SBF. The phosphate bands are indicated.

the material formed on the surface of the pellets after 0, 3, 7 and 15 days of immersion in SBF were included in the Fig. 6(g). It is possible identify some bands characteristic of the apatite phases. The bands that appear around 570 to 600 cm^{-1}, which become more intense as the immersion time in SBF increases, can be assigned to the absorption modes of the PO_4 groups of calcium phosphates, indicating the incipient formation of this material on the surface of the samples. Similarly, it is possible to identify a peak around 1040 cm^{-1} also associated with phosphate groups. The band at 1450 cm^{-1} is assigned to the stretching of CO_3^{2-} [33]. There is no good definition in the bands because the process of formation of the apatite layer begins with the formation of amorphous materials. The formation of this kind of apatitic layer is a necessary condition for a material to bind to living tissue when implanted. Based on this, it can be stated that scaffolds with calcium phosphate particles are potentially bioactive [23, 47, 48, 51].

Biological tests

Cytotoxicity

Figure 7(a) shows the cell viability results obtained by MTT of the L929 culture exposed to the 0CaP material. For the 4 types of extracts made, viability is not affected and is very similar to the negative control and cells, with values close to 100% viability. Likewise, the cell viability of the culture exposed to the different concentrations of the 05CaP and 1CaP materials [Fig. 7(b) and (c)] respectively, do not present variations in comparison with the controls. This indicates that neither the polymeric material or the polymer-ceramic compound is toxic to these cells and provide a favorable environment for their growth and proliferation. Figure 7(d) shows the comparison of cell viability between the highest concentrations of the different scaffolds, showing that there are no significant differences between them. From this, it can be concluded that the presence of a greater number of ceramic nanoparticles does not affect the biocompatibility of the material.

Figure 8 presents the photographs of the cell cultures exposed to the positive and negative controls and to the materials with different concentrations of calcium phosphate particles. Figure 8(a) and (b) show the elongated morphology typical of L929 cells when they are in an environment that guarantees their proper growth and adhesion to the dish when in contact with a non-toxic material (negative control). These photographs show the conditions of a culture in which viability is not affected, since the morphology does not change and there is a high confluence in the dish. On the contrary, in Fig. 8(c) dead cells that are circular in shape and detached from the dish can be observed. This is due to their proximity to a toxic material (positive control), which produces an inhibition halo on its periphery i.e., an area where there are no living cells around the cytotoxic material. Figures 8(d–f) show the appearance of the cell culture after 3 days in contact with the scaffolds 0CaP [Fig. 8(d)], 05CaP [Fig. 8(e)], and 1CaP [Fig. 8(f)]. It can be observed that the morphology of the cells does not change, and they do not detach

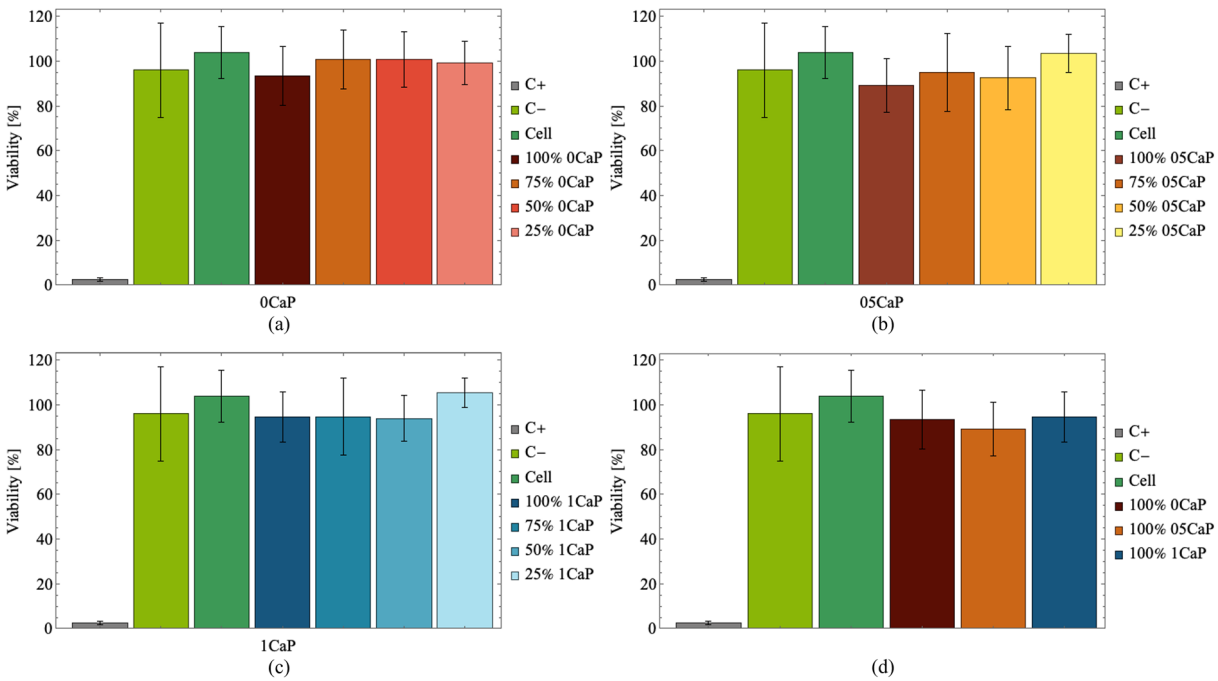

Figure 7: Cell viability with extracts at 100, 75, 50, and 25% V/V of extracts in cellular medium (a) 0CaP (b) 05CaP, and (c) 1CaP. (d) Comparison between scaffolds 0CaP, 05CaP, and 1CaP at maximum extract concentration.

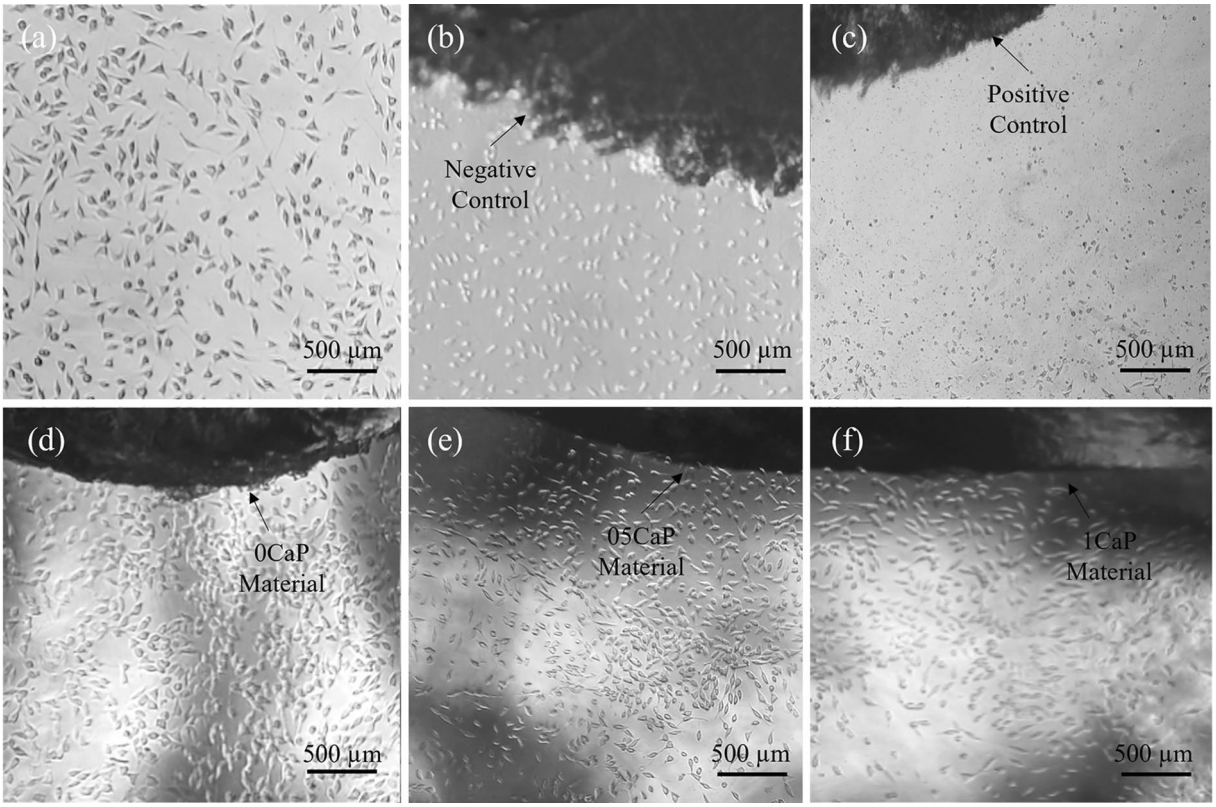

Figure 8: Light microscopy photographs of the in vitro inhibition halo cytotoxicity assay. (a) Control of cells. (b) Negative control. (c) Positive control. (d) Scaffold 0CaP (e) Scaffold 05CaP. (f) 1CaP scaffold. All the images are at 50×.

from the plate or die when in contact with the different scaffolds. Therefore, the formation of an inhibition halo is not observed. Hence, the biocompatibility of the materials with which the scaffolds were manufactured, regardless of their ceramic load, is once again confirmed. This result is comparable with those of Guillaume et al. [52] where different ceramic loads within a polymeric resin did not affect cytotoxicity.

Cell adhesion test

Once the test started, the cells deposited in each scaffold could be observed both on the scaffold and in the surrounding area. The cells had rounded morphology, which is characteristic of not adhering to any surface. Over time, a greater number of cells adhering to the surface of the scaffolds could be observed, which presented elongated shapes, [Fig. 9(a), (c), (e)]. On the third day, although a noticeable increase in the number of cells was not observed, some differences could be seen in the number of cells on the surface of the 05CaP and 1CaP scaffolds compared to those of 0CaP. The sites where the greatest number of adhered cells were observed were the areas of the gyroid geometry with much more pronounced curves and in the more internal spaces of the scaffolds. When observing the scaffolds on the eighth day by scanning electron microscopy (SEM) [Fig. 9(b), (d) and (f)], it could be seen that the number of cells had increased, being significantly higher in the 05CaP and 1CaP scaffolds than in those of 0CaP. The cells observed had elongated shapes and were interconnected with each other.

The cells almost filled the surface of the scaffolds that contained ceramic loads, with large cell conglomerates in the curved zones of the pores of the gyroid geometry. In previous work, the authors verified that geometry with interconnected porosity favors cell adhesion [8]. Other authors have highlighted the importance of geometries like gyroid in biological behaviour of the scaffolds [53]. Similar results were also found by Gauvin et al. [54], who found that when making porous structures by the stereolithography technique, the interconnectivity of the pores favors the proliferation and uniform distribution of human umbilical vein endothelial cells (HUVEC) in the scaffolding. It has also been verified in several studies that the presence of calcium phosphate particles promotes cell proliferation [21, 26, 55–57]. However, no reports have been found of works where cell adhesion is studied in scaffolds with different concentrations of calcium phosphate particles in a polymeric resin matrix. In addition, it was found in this study that surface treatment with oxygen plasma, which promotes the formation of polar functional

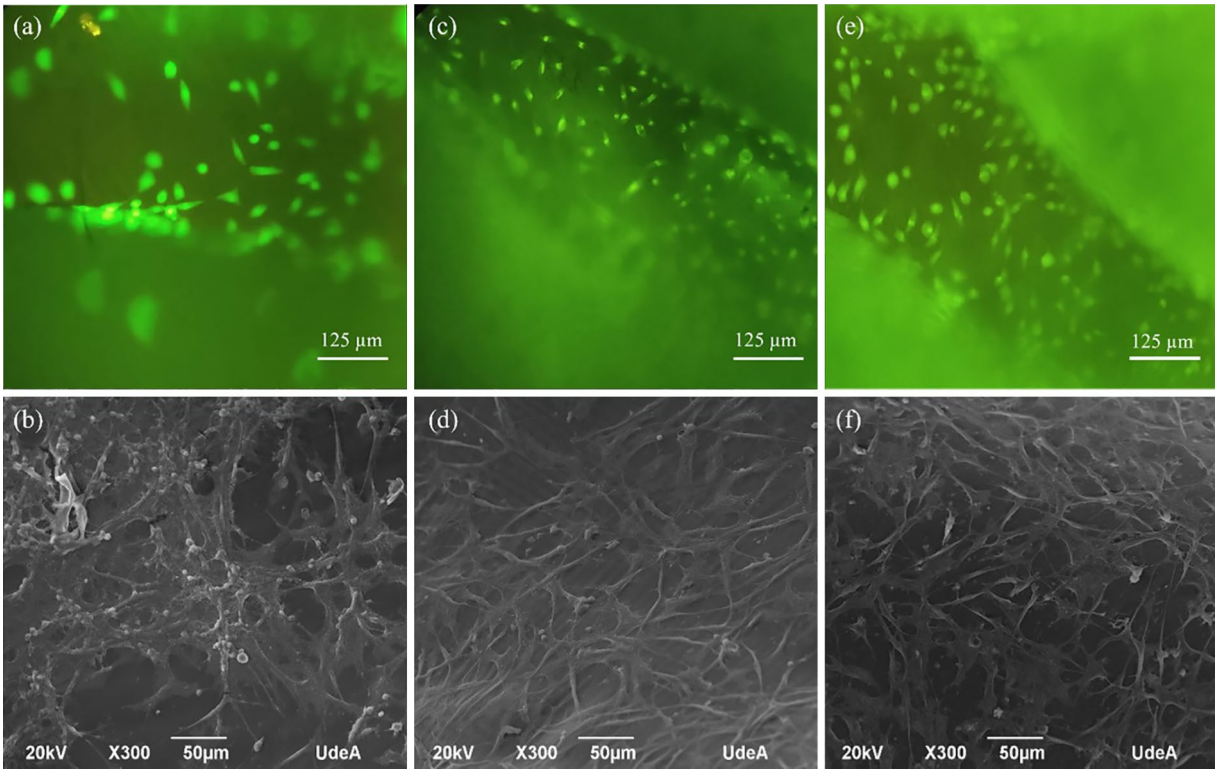

Figure 9: Fluorescence microscopy images of the scaffolds subjected to the cell adhesion assay after three days. (a) 0CaP scaffolds, (c) 05CaP scaffolds, (e) 1CaP scaffolds. All the fluorescence images at 200× and scanning electron microscopy (SEM) images after 8 days of assay (b) 0CaP scaffolds, (d) 05CaP scaffolds, and (f) 1CaP scaffolds.

groups, facilitates cell adhesion to the walls of the scaffolds. Moreover, this remained stable over time, since after eight days the cells continued to adhere and grow.

Conclusions

In the present work, scaffolds with gyroid TPMS geometry were developed through the DLP 3D printing technique with a commercial resin of acrylic nature and loaded with calcium phosphate nanoparticles at 0.5% and 1% w/V. the printing of a composite material was achieved and demonstrated that with these amounts of particles there is no interference with the light so that the printing is fast and efficient. The resin presented behavior typical of an acrylic resin in the TGA test and a low viscosity, making it suitable for printing. The scaffolds were analyzed by scanning electron microscopy, verifying the regularity and precision of the surfaces of the scaffolds obtained with DLP technology. The presence of ceramic particles in the bodies formed was also verified, with a higher content in the scaffolds with 1CaP than those with 05CaP or 0CaP. The mechanical strength to compression tests carried out on the scaffolds confirmed that the presence of ceramic particles in the scaffolds did not affect their mechanical behavior, making them suitable for use in biomedical applications. The surface treatment by oxygen plasma carried out on the samples resulted in a remarkable improvement in the wettability of the surfaces, which is a favorable condition for cell adhesion, whereby this technique can be considered in cases where is going to be use a polymer or composite with a considerable hydrophobicity for biological applications to improve the wettability. The in vitro bioactivity test showed that, in contact with SBF, the resin-ceramic composite forms an apatitic layer from the third day of exposure, indicating its in vitro bioactive behavior. This result was corroborated by biological tests, where it was shown that the material is not cytotoxic and favors cell adhesion, biologically, there is no significant difference with particles, which means that with only 0.5% w/V of particles the resin is bioactive and the response with cells is favorable. however, it is possible to evaluate the behavior with a greater number of particles in future work, to determine a concentration where the adhesion is higher and faster so that the material is enhanced for more permanent bone repairs. Additionally, as in previous work was demonstrated, it was verified that the gyroid geometry promotes cell proliferation, since the characteristic curves of this geometry were the sites of highest cell concentration in the cellular adhesion test.

Materials and methods

Resin and calcium phosphate particles

For the manufacturing of the scaffolds by stereolithography, the commercial resin *Portux Print 3D Model* without pigment (New Stetic) was used. The calcium phosphate particles used in the resin-ceramic suspension that served as raw material in the printing of the samples were obtained by the solution self-combustion method [28]. Calcium nitrate tetrahydrate $Ca(NO_3)_24H_2O$ (Merck) was used as a calcium source and diammonium hydrogen phosphate $(NH_4)2HPO_4$ (Alfa Aesar) was used as a phosphorus source. Glycine $C_2H_5NO_2$ (Merck) was used as fuel and 65% nitric acid HNO_3 (Biochemical) as a catalyst. The powders obtained were characterized in terms of their structure and morphology. The results of which were published in previous work [28]. In order to avoid agglomerates the particles were subjected to grinding in a ball mill (Retsch PM 100) for 20 min at 200 rpm with intervals of 5 min and rotation reversal, before being mixed with the resin.

Suspension of calcium phosphate particles in the resin.

The commercial resin was subjected to several characterizations. Thermogravimetry (TGA) was performed on a specimen of cured resin in a TA Instruments Discovery 550 device with an air atmosphere and a heating ramp of 10 °C/min up to 1000 °C. Fourier transform infrared (FTIR) spectroscopy was performed in a Shimadzu IRTracer-100 device with an accessory to measure transmittance, before and after curing. The spectra were acquired in a spectral range of 500–4000 cm^{-1}. The viscosity of the liquid resin was measured at room temperature (approximately 25ºC) with a rotational viscometer (LCD digital NDJ-8S) at a speed of 60 rpm with a #3 rotor.

Suspensions with concentrations of 0% (0CaP), 0.5% (05CaP), and 1% (1CaP) w/V of calcium phosphate particles were used. The amount of resin required for the preparation of each batch was placed in a beaker. To achieve this, the nanoparticles were gradually added while mixing with a high-shear mixer (Heidolph) for 3 min to homogenize the mixture, avoiding large bubbles that could affect printing and drastic temperature increases that could trigger unwanted polymerization processes.

Obtention of the scaffolds

The 3D printer used was a *Wanhao Duplicator 7* (Wanhao) that works by digital light processing (DLP) with a 405 nm wavelength light source. The CAD file, which contained the prototype, underwent a slicing process. This information is sent to the machine which, using masks, projects each section or plane onto the liquid resin. The mobile platform of the machine is located in the lower part of the *z*-axis. It is submerged in the vat with resin, leaving a thin bed of material between itself and the bottom of the container that solidifies when the light hits it, giving the shape of the layer. The platform rises with the solidified resin mechanically adhered to it, before being submerged at the bottom of the container once again. The process is repeated as many times as necessary until all the layers have been solidified one on top of the other and an object with the designed geometry is obtained.

The TPMS selected for the scaffold geometry was a gyroid with an external cylindrical shape. The interconnected pores circuits of TPMS structures can be described through trigonometric functions, and these were modelled using MathMod® software in previous work [51]. Initially The unit cell of each TPMS was obtained, which was replicated in three dimensions, 5 times in each XYZ coordinate axis so that the resulting surfaces consisted of 125 unit cells total [51]. From the modelled surfaces, Chitubox software (CBC-Tech) was used to impart the final dimensions to these. The solids were designed with a wall thickness of 0.5 mm and overall dimensions of $10 \times 10 \times 5$ mm^3. The figure was designed for a porosity of 80%. Also, 10 mm diameter and 2 mm high pill-shaped specimens were printed and used for contact angle measurements, in vitro bioactivity, and thermal tests. The printing and slicing parameters were configured using too the Chitubox software (CBD-Tech), with a layer thickness of 0.045 mm and exposure times of 43 s for the lower layers and 20 s for the other layers, in the case of scaffolds, and 43 s for all layers in the case of the pills. Once the samples were printed, they were cleaned for 3 min using isopropyl alcohol and post-cured with a *Next Dent LC-3D Print Box* camera at a wavelength between 300 and 550 nm for 10 min.

To decrease the hydrophobicity and improve the wettability of the samples, the surface of the scaffolds and pellets were subjected to treatment with oxygen plasma in a PLASMA CLEANER PDC-32G Harrick plasma unit, exposing them for 4 min at maximum intensity on each side.

Characterization of the samples.

Scaffolds with and without calcium phosphate particles were characterized by scanning electron microscopy (SEM). For this, the samples were fixed on a graphite tape, thinly coated in gold (Au) (DENTON VACUUM desk IV) and analyzed in the scanning electron microscope (JEOL JSM 6490 LV, JEOL, Germany) in a high vacuum to obtain high-resolution images. The secondary electron detector was used to evaluate the morphology and topography of the samples. Elemental analysis was performed using an EDX-X-ray microprobe (INCA PentaFETx3, Oxford Instruments, UK). Additionally, the scaffolds with diameter

of 10 mm and a height of 5 mm were subjected to monotonic compressive tests using a universal testing machine (Instron 3366, Instron, MA, USA) with a constant displacement rate of 0.001 mm/s. Measurements were taken in 5 scaffolds of each type under the same conditions.

The tablets with and without plasma surface treatment were subjected to contact angle measurement, using a Dataphysics device, OCA 15 EC, and analyzing the data through the ORCA program. The purpose of this was to verify the variation and the improvement in the wettability of the material. For this, measurements were taken at 3 different points of the same sample, applying a drop of distilled water with a dosage of 1 µL.

In vitro bioactivity assay

A material is considered bioactive when it has the ability to induce the formation of connective tissue on its surface through an apatitic layer that is generated when it is in contact with physiological fluids and which in turn promotes bonding with the living tissue [44, 47, 48, 58]. To test the in vitro bioactivity, simulated body fluid (SBF) prepared as indicated by Kokubo et al. [23, 49, 59] was used, using Tris(hydroxymethyl)aminomethane, 99.9 + % (Aldrich) and HCl concentrate as a buffer. Pills with a diameter of 10 mm of each of the compounds obtained with the different concentrations of calcium phosphate particles were independently suspended in sealed polyethylene containers containing 20 mL of SBF at pH 7.25–7.35 and 37 °C. The ratio of the exposed area of the sample to fluid volume was 0.3 cm^2/mL. The samples were submerged for periods of up to 18 days. Every day one sample was removed from its respective container, washed with distilled water, and dried at room temperature. Analysis of the surface and the presence of the apatitic phase were performed by means of Fourier transform infrared (FTIR) spectroscopy performed in a Shimadzu IRTracer-100 and scanning electron microscopy (SEM). The samples were fixed on a graphite tape, thinly coated in gold (Au) (DENTON VACUUM desk IV) and analyzed in a scanning electron microscope (JEOL JSM 6490 LV, JEOL, Germany) in a high vacuum. Elemental analysis was performed using an EDX-X-ray microprobe (INCA PentaFETx3, Oxford Instruments, UK).

Biological assays

Cytotoxicity test

A cytotoxicity test with MTT was performed according to ISO 10993-5-2009 *Biological evaluation for medical* [60] *devices*. 96-well plates were used. Initially, 10,000 cells of the L929 cell line (NCTC clone 929 [L cell, L-929, derivative of Strain L]) ATCC Nr. CCL-1 were seeded in each well, using DMEM:F12 (Lonza, Switzerland) as medium at 10% V/V of fetal bovine serum (Gibco, USA). Dimethyl sulfoxide (Merck, Germany) at 10% V/V was used as a positive control, and an extract from the tip of a micropipette previously sterilized with ethylene oxide gas was used as a negative control. As an additional control, a well was kept with only cells in its medium. Extracts were prepared from each scaffold (0CaP, 05CaP, and 1CaP), previously sterilized with ethylene oxide gas, and from the micropipette tip following a ratio of 1 mL of medium per mg of weight. On the second day, the medium was removed, and the extracts made with the different scaffolds were deposited in the wells at concentrations of 100%, 75%, 50%, and 25% V/V of extract in cellular medium. Each of these, as well as the controls and blank, were done in triplicate. On the final day (the third), the extracts were removed, 50 µL of MTT (Alfa Aesar, USA) were added to each well and, after 2 h the absorbance compared to the blanks was measured with a wavelength of 570 nm. As a variation to the protocol, the MTT was prepared at 1 mg/mL in lactated Ringer's (Baxter, USA). The test was performed three times, each time in triplicate with each type of scaffold. To determine the percentage of cell viability, Eq. (1) presented in the standard ISO 10993- 5 [60] was used. Where OD_{570e} is the measured value of the optical density of the sample extracts at 100% and OD_{570b} is the measured value of the optical density of the blank, understood in this case as the positive control.

$$\text{Cellviability}(\%) = \frac{100 \times OD_{570e}}{OD_{570b}} \quad (1)$$

The cytotoxicity results were corroborated through a contact test based on the ISO 10993-5 standard [60], with the L929 cell line, verifying the appearance of inhibition halos around the scaffolds. As positive and negative controls, pieces of filter paper sterilized with ethylene oxide were used, with 4 µL of dimethyl sulfoxide for the positive cases. 6-well plates were used. On the first day in each well, 300,000 cells were seeded in DMEM:F12 medium (Lonza, Switzerland) at 10% V/V of fetal bovine serum (Gibco, USA). On the second day, after confirming a confluence of 80%, the different types of scaffolds, previously sterilized, were glued into the center of the well with commercial glue. The commercial glue's innocuousness was previously verified by means of a contact test, and the medium was added again until the scaffold was completely covered. On the third day, the wells were observed under a microscope (Leica, Germany), and the presence of inhibitory halos around the composite material was determined and characterized. The test was performed in triplicate with each type of scaffold.

Cell adhesion test

To evaluate the adhesion of the L929 cell line in the scaffolds with the different concentrations of calcium phosphate particles superficially treated with oxygen plasma, the scaffolds were placed in a 6-well plate without treatment on which

100,000 cells were deposited. The dish was placed in an incubator for 2 h, and after that, 3 mL of culture medium was added before incubating again. The experiment was kept under observation for 8 days. On the third day, the cells were stained with a solution of calcein (Life Technologies, USA) and dimethylsulfoxide to obtain images by fluorescence microscopy. A working solution based on Ringer's lactate (Corpaul, Colombia) was prepared, which consisted of a ratio of 2 µL of previously prepared calcein for each mL of Lactate. The medium from each dish was discarded and washed with Ringer's lactate, and 500 µL of the working solution was added to each scaffold. It was left to incubate for 30 min, after which scaffolds were observed under a microscope with a UV light source. The scaffolds were again left with 3 mL of medium in the incubator until the remaining time was completed.

On the eighth day, the cells were fixed in the scaffolds for observation by scanning electron microscopy. The fixation process took 3 days. On the first day, the medium from each dish was discarded, the dish was washed 3 times with Ringer's lactate, and 4 mL of 10% formaldehyde (Merck, Germany) was added to each one, leaving it completely covered in the laminar flow cabinet for 24 h. On the second day, the solution was discarded, and the dishes were washed with water (Corpaul, Colombia) 3 times, adding 4 mL of 3% glutaraldehyde (Merck, Germany) to each well and leaving it completely covered for 24 h in the laminar flow cabinet. Finally, on the third day, the solution from the previous day was discarded, the dishes were washed 3 times with water and the dehydration process was carried out using ethanol at different concentrations (30, 50, 70, 95, 99% V/V) for times of up to 43 min. At the last concentration, each scaffold was left to dry completely at room temperature. Subsequently, the samples were fixed on a graphite strip, previously coated with a thin layer of gold (Au) and observed by a scanning electron microscope (SEM) (JEOL JSM 6490 LV, JEOL, Germany) in high vacuum (DENTON VACUUM desk IV). The test was performed in triplicate with each type of scaffold.

Acknowledgments

This work was partially supported by the project Hermes code 57524 from Universidad Nacional de Colombia.

Author contributions

LMR, SO and CG contributed to conceptualization; CD, CG, SO, LMA, LMR, AO and CG contributed to formal analysis and investigation; CD and CG contributed to writing-original draft preparation; LMR and CG contributed to supervision; AFV provided some additional suggestions on experiments.

Funding

Open Access funding provided by Colombia Consortium. This work was partially supported by the project Hermes code 57524 from Universidad Nacional de Colombia.

Data availability

The data that support the findings of this study are available within the article. There is no data that needs to be stored and presented.

Code availability

Not applicable.

Declarations

Conflict of interest The authors declare that they have not conflict of interest.

Ethical approval

This study doesn't contain any studies with human or animal subjects perform by any of the authors.

Open Access

References

1. L.A. González, G.M. Vásquez, J.F. Molina, Epidemiología de la osteoporosis. Rev. Clin. Esp. **16**, 15 (2009)
2. N. Abbasi, S. Hamlet, R.M. Love, N.-T. Nguyen, Porous scaffolds for bone regeneration. J. Sci. **5**, 1–9 (2020). https://doi.org/10.1016/j.jsamd.2020.01.007
3. L.J. Melton, Hip fractures: a worldwide problem today and tomorrow. Bone **14**, 1–8 (1993). https://doi.org/10.1016/8756-3282(93)90341-7

4. H. Yi, F. Ur Rehman, C. Zhao et al., Recent advances in nano scaffolds for bone repair. Bone Res. **4**, 16050 (2016). https://doi.org/10.1038/boneres.2016.50
5. B. Felice, M.A. Sánchez, M.C. Socci et al., Controlled degradability of PCL-ZnO nanofibrous scaffolds for bone tissue engineering and their antibacterial activity. Mater. Sci. Eng. C **93**, 724–738 (2018). https://doi.org/10.1016/j.msec.2018.08.009
6. M. Ribeiro, M.P. Ferraz, F.J. Monteiro et al., Antibacterial silk fibroin/nanohydroxyapatite hydrogels with silver and gold nanoparticles for bone regeneration. Nanomedicine **13**, 231–239 (2017). https://doi.org/10.1016/j.nano.2016.08.026
7. O. Guillaume, M.A. Geven, C.M. Sprecher et al., Surface-enrichment with hydroxyapatite nanoparticles in stereolithography-fabricated composite polymer scaffolds promotes bone repair. Acta Biomater. **54**, 386–398 (2017). https://doi.org/10.1016/j.actbio.2017.03.006
8. J.A. Ramírez, V. Ospina, A.A. Rozo et al., Influence of geometry on cell proliferation of PLA and alumina scaffolds constructed by additive manufacturing. J. Mater. Res. **34**, 3757–3765 (2019). https://doi.org/10.1557/jmr.2019.323
9. B. Dhandayuthapani, Y. Yoshida, T. Maekawa, D.S. Kumar, Polymeric scaffolds in tissue engineering application: a review. Int. J. Polym. Sci. **2011**, 1–19 (2011). https://doi.org/10.1155/2011/290602
10. R. Ambu, A. Morabito, Porous scaffold design based on minimal surfaces: development and assessment of variable architectures. Symmetry **10**, 361 (2018). https://doi.org/10.3390/sym10090361
11. H. Zhang, C. Jiao, Z. Liu et al., 3D-printed composite, calcium silicate ceramic doped with CaSO4·2H2O: degradation performance and biocompatibility. J. Mech. Behav. Biomed. Mater. **121**, 104642 (2021). https://doi.org/10.1016/j.jmbbm.2021.104642
12. I. Gibson, D. Rosen, B. Stucker, *Additive Manufacturing Technologies* (Springer, New York, 2015)
13. F.P.W. Melchels, J. Feijen, D.W. Grijpma, A review on stereolithography and its applications in biomedical engineering. Biomaterials **31**, 6121–6130 (2010). https://doi.org/10.1016/j.biomaterials.2010.04.050
14. S. Bose, S. Vahabzadeh, A. Bandyopadhyay, Bone tissue engineering using 3D printing. Mater. Today **16**, 496–504 (2013). https://doi.org/10.1016/j.mattod.2013.11.017
15. A. Ronca, L. Ambrosio, D.W. Grijpma, Preparation of designed poly(d, l-lactide)/nanosized hydroxyapatite composite structures by stereolithography. Acta Biomater. **9**, 5989–5996 (2013). https://doi.org/10.1016/j.actbio.2012.12.004
16. R. Palucci Rosa, G. Rosace, Nanomaterials for 3D printing of polymers via stereolithography: concept, technologies, and applications. Macromol. Mater. Eng. **306**, 2100345 (2021). https://doi.org/10.1002/mame.202100345
17. J.Y. Kim, J.W. Lee, S.-J. Lee et al., Development of a bone scaffold using HA nanopowder and micro-stereolithography technology. Microelectron. Eng. **84**, 1762–1765 (2007). https://doi.org/10.1016/j.mee.2007.01.204
18. A. Al Rashid, S.A. Khan, G.S. Al-Ghamdi, Koç M, Additive manufacturing of polymer nanocomposites: needs and challenges in materials, processes, and applications. J. Market. Res. **14**, 910–941 (2021). https://doi.org/10.1016/j.jmrt.2021.07.016
19. J.R.C. Dizon, A.H. Espera, Q. Chen, R.C. Advincula, Mechanical characterization of 3D-printed polymers. Addit. Manuf. **20**, 44–67 (2018). https://doi.org/10.1016/j.addma.2017.12.002
20. G. Taormina, C. Sciancalepore, M. Messori, F. Bondioli, 3D printing processes for photocurable polymeric materials: technologies, materials, and future trends. J. Appl. Biomater. Funct. Mater. **16**, 151–160 (2018). https://doi.org/10.1177/2280800018764770
21. X. Li, Y. Yuan, L. Liu et al., 3D printing of hydroxyapatite/tricalcium phosphate scaffold with hierarchical porous structure for bone regeneration. Bio-des Manuf. **3**, 15–29 (2020). https://doi.org/10.1007/s42242-019-00056-5
22. H. Zhu, M. Li, X. Huang et al., 3D printed tricalcium phosphate-bioglass scaffold with gyroid structure enhance bone ingrowth in challenging bone defect treatment. Appl. Mater. Today **25**, 101166 (2021). https://doi.org/10.1016/j.apmt.2021.101166
23. C. Ohtsuki, Mechanism of apatite formation on CaO-SiO2-P205 glasses in a simulated body fluid. J. Non-Crystal. Solids **143**, 84–92 (1992)
24. M. Ly, S. Spinelli, S. Hays, D. Zhu, 3D Printing of Ceramic Biomaterials. Eng. Regen. **3**, 41–52 (2022). https://doi.org/10.1016/j.engreg.2022.01.006
25. A.V.M. Esteves, M.I. Martins, P. Soares et al., Additive manufacturing of ceramic alumina/calcium phosphate structures by DLP 3D printing. Mater. Chem. Phys. **276**, 125417 (2022). https://doi.org/10.1016/j.matchemphys.2021.125417
26. S. Liu, L. Mo, G. Bi et al., DLP 3D printing porous β-tricalcium phosphate scaffold by the use of acrylate/ceramic composite slurry. Ceram. Int. **47**, 21108–21116 (2021). https://doi.org/10.1016/j.ceramint.2021.04.114
27. C. Feng, K. Zhang, R. He et al., Additive manufacturing of hydroxyapatite bioceramic scaffolds: dispersion, digital light processing, sintering, mechanical properties, and biocompatibility. J. Adv. Ceram. **9**, 360–373 (2020). https://doi.org/10.1007/s40145-020-0375-8
28. A.A. Lopera, A. Montoya, I.D. Vélez et al., Synthesis of calcium phosphate nanostructures by combustion in solution as a potential encapsulant system of drugs with photodynamic properties for the treatment of cutaneous leishmaniasis. Photodiagn. Photodyn. Ther. **21**, 138–146 (2018). https://doi.org/10.1016/j.pdpdt.2017.11.017
29. A.A. Lopera, E.A. Chavarriaga, B. Zuluaga et al., Effect of salt concentration on the electrical and morphological properties of calcium phosphates obtained via microwave-induced combustion synthesis. Adv. Powder. Technol. **28**, 2787–2795 (2017). https://doi.org/10.1016/j.apt.2017.08.007

30. A. Lopera, E.A. Chavarriaga, V.D.N. Bezzon et al., Synthesis of high crystallinity biphasic calcium phosphates/gold nanoparticles composites by solution combustion method with antimicrobial response. Boletín de la Sociedad Española de Cerámica y Vidrio **61**, 487–497 (2022). https://doi.org/10.1016/j.bsecv.2021.03.007
31. M. Canillas, P. Pena, A.H. de Aza, M.A. Rodríguez, Calcium phosphates for biomedical applications. Boletín de la Sociedad Española de Cerámica y Vidrio **56**, 91–112 (2017). https://doi.org/10.1016/j.bsecv.2017.05.001
32. S. Zakeri, M. Vippola, E. Levänen, A comprehensive review of the photopolymerization of ceramic resins used in stereolithography. Addit. Manuf. **35**, 101177 (2020). https://doi.org/10.1016/j.addma.2020.101177
33. Z. Hassan, N. Hatim, A. Taqa, Study the FTIR of Hydroxyapatite Additive to Heat Cured Acrylic Resin. Al-Rafidain Dental J. **14**, 32–36 (2014). https://doi.org/10.33899/rden.2014.89250
34. Y. Qiu, N. Zhang, Q. Kang et al., Chemically modified light-curable chitosans with enhanced potential for bone tissue repair. J. Biomed. Mater. Res. **89A**, 772–779 (2009). https://doi.org/10.1002/jbm.a.32017
35. B.W. Huang, G.L. Cheng, C. Deng, H.H. Zou, Investigation on some properties of renshape™ SL7545 type photosensitive resin and its application for stereolithography material. AMM **252**, 220–223 (2012). https://doi.org/10.4028/www.scientific.net/AMM.252.220
36. X. Zhang, Y. Xu, L. Li et al., Acrylate-based photosensitive resin for stereolithographic three-dimensional printing. J. Appl. Polym. Sci. **136**, 47487 (2019). https://doi.org/10.1002/app.47487
37. B.W. Huang, M.Y. Chen, Evaluation on some properties of SL7560 type photosensitive resin and its fabricated parts. AMM **117–119**, 1164–1167 (2011). https://doi.org/10.4028/www.scientific.net/AMM.117-119.1164
38. B. Huang, Z. Du, T. Yong, W. Han, Preparation of a novel hybrid type photosensitive resin for stereolithography in 3D printing and testing on the accuracy of the fabricated parts. J. Wuhan Univ. Technol-Mat. Sci. Edit **32**, 726–732 (2017). https://doi.org/10.1007/s11595-017-1659-x
39. Z. Liu, H. Liang, T. Shi et al., Additive manufacturing of hydroxyapatite bone scaffolds via digital light processing and in vitro compatibility. Ceram. Int. **45**, 11079–11086 (2019). https://doi.org/10.1016/j.ceramint.2019.02.195
40. Y. Wang, S. Chen, H. Liang et al., Digital light processing (DLP) of nano biphasic calcium phosphate bioceramic for making bone tissue engineering scaffolds. Ceram. Int. **48**, 27681–27692 (2022). https://doi.org/10.1016/j.ceramint.2022.06.067
41. C. Goutagny, S. Hocquet, D. Hautcoeur et al., Development of calcium phosphate suspensions suitable for the stereolithography process. Open Ceram. **7**, 100167 (2021). https://doi.org/10.1016/j.oceram.2021.100167
42. J.R. Caeiro, P. González, D. Guede, Biomecánica y hueso (y II): ensayos en los distintos niveles jerárquicos del hueso y técnicas alternativas para la determinación de la resistencia ósea. Rev. Osteoporos. Metab. Miner. **5**, 99–108 (2013). https://doi.org/10.4321/S1889-836X2013000200007
43. K. Dave, Z. Mahmud, V.G. Gomes, Superhydrophilic 3D-printed scaffolds using conjugated bioresorbable nanocomposites for enhanced bone regeneration. Chem. Eng. J. **445**, 136639 (2022). https://doi.org/10.1016/j.cej.2022.136639
44. A. Rámila, Vallet-Regí M, Static and dynamic in vitro study of a sol–gel glass bioactivity. Biomaterials **22**, 2301–2306 (2001). https://doi.org/10.1016/S0142-9612(00)00419-1
45. P. Alves, S. Pinto, H.C. de Sousa, M.H. Gil, Surface modification of a thermoplastic polyurethane by low-pressure plasma treatment to improve hydrophilicity. J. Appl. Polym. Sci. **122**, 2302–2308 (2011). https://doi.org/10.1002/app.34348
46. V. Raeisdasteh Hokmabad, S. Davaran, A. Ramazani, R. Salehi, Design and fabrication of porous biodegradable scaffolds: a strategy for tissue engineering. J. Biomater. Sci. Polym. Ed. **28**, 1797–1825 (2017). https://doi.org/10.1080/09205063.2017.1354674
47. P. Li, C. Ohtsuki, T. Kokubo et al., Apatite formation induced by silica gel in a simulated body fluid. J. Am. Ceramic Soc. **75**, 2094–2097 (1992). https://doi.org/10.1111/j.1151-2916.1992.tb04470.x
48. P. Li, C. Ohtsuki, T. Kokubo et al., Process of formation of bone-like apatite layer on silica gel. J. Mater. Sci. **4**, 127–131 (1993). https://doi.org/10.1007/BF00120381
49. T. Kokubo, H.-M. Kim, M. Kawashita, Novel bioactive materials with different mechanical properties. Biomaterials **24**, 2161–2175 (2003). https://doi.org/10.1016/S0142-9612(03)00044-9
50. Z. Amjad, *Calcium Phosphates in Biological and Industrial Systems* (Springer Science & Business Media, New York, 2013)
51. S. Restrepo, S. Ocampo, J.A. Ramírez et al., Mechanical properties of ceramic structures based on Triply Periodic Minimal Surface (TPMS) processed by 3D printing. J. Phys. Conf. Ser. **935**, 012036 (2017). https://doi.org/10.1088/1742-6596/935/1/012036
52. O. Guillaume, M.A. Geven, D.W. Grijpma et al., Poly(trimethylene carbonate) and nano-hydroxyapatite porous scaffolds manufactured by stereolithography: composite PTMC/HA scaffold using stereolithography. Polym. Adv. Technol. **28**, 1219–1225 (2017). https://doi.org/10.1002/pat.3892
53. M.E. Dokuz, M. Aydın, M. Uyaner, Production of bioactive various lattices as an artificial bone tissue by digital light processing 3D printing. J. Mater. Eng. Perform. **30**, 6938–6948 (2021). https://doi.org/10.1007/s11665-021-06067-7
54. R. Gauvin, Y.-C. Chen, J.W. Lee et al., Microfabrication of complex porous tissue engineering scaffolds using 3D

projection stereolithography. Biomaterials **33**, 3824–3834 (2012). https://doi.org/10.1016/j.biomaterials.2012.01.048

55. G. Bi, L. Mo, S. Liu et al., DLP printed β-tricalcium phosphate functionalized ceramic scaffolds promoted angiogenesis and osteogenesis in long bone defects. Ceram. Int. **48**, 26274–26286 (2022). https://doi.org/10.1016/j.ceramint.2022.05.310
56. Z. Wang, C. Huang, J. Wang et al., Design and characterization of hydroxyapatite scaffolds fabricated by stereolithography for bone tissue engineering application. Procedia CIRP **89**, 170–175 (2020). https://doi.org/10.1016/j.procir.2020.05.138
57. Y. Zeng, Y. Yan, H. Yan et al., 3D printing of hydroxyapatite scaffolds withgood mechanical and biocompatible properties by digital light processing. J. Mater. Sci. **53**, 6291–6301 (2018). https://doi.org/10.1007/s10853-018-1992-2
58. C. Ohtsuki, T. Kokubo, T. Yamamuro, Mechanism of apatite formation on CaO-SiO2-P205 glasses in a simulated body fluid. J. Non Cryst. Solids **143**, 84–92 (1992)
59. C. Ohtsuki, T. Kokubo, T. Yamamuro, Compositional dependence of bioactivity of glasses in the system CaO-SiO2-AI203: its in vitro evaluation. J. Mater. Sci. **3**, 119–125 (1992)
60. International Organization for Standardization. ISO 10993-5:2009 Biological evaluation of medical devices—Part 5: Tests for in vitro cytotoxicity (2009).